How to prove that a $\not{E}_T$ excess at the LHC is not due to dark matter

Doojin Kim[1] and Konstantin T. Matchev[2]
[1]Theoretical Physics Department, CERN, CH-1211 Geneva 23, Switzerland
[2]Physics Department, University of Florida, Gainesville, Florida 32611, USA

(Received 2 February 2018; revised manuscript received 14 May 2018; published 14 September 2018)

If the LHC is able to produce dark matter particles, they would appear at the end of cascade decay chains, manifesting themselves as missing transverse energy. However, such "dark matter candidates" may themselves decay invisibly. We propose to test for this possibility by studying the effect of particle widths on the observable invariant mass distributions of the visible particles seen in the detector. We consider the simplest nontrivial case of a two-step two-body cascade decay and derive analytically the shapes of the invariant mass distributions, for generic values of the widths of the new particles. We demonstrate that the resulting distortion in the shape of the invariant mass distribution can be significant enough to measure the width of the dark matter "candidate," ruling it out as the source of the cosmological dark matter.

DOI: 10.1103/PhysRevD.98.055018

I. INTRODUCTION

Events with missing transverse energy, $\not{E}_T$, at the Large Hadron Collider (LHC) at CERN could be indicative of the production of dark matter particles; the latter are stable and weakly interacting, and, once produced in the collision, will escape without leaving a trace inside the detector. This causes an imbalance in the transverse momentum of the event, $\vec{\not{p}}_T$, whose magnitude is colloquially known as the "missing transverse energy," $\not{E}_T = |\vec{\not{p}}_T|$. However, the reverse statement is not so obvious: if we observe an excess of $\not{E}_T$ events at the LHC, how can one be sure that what we are seeing is indeed *the* cosmological dark matter?

The question of *proving* that a $\not{E}_T$ signal observed at the LHC is indeed due to dark matter, has attracted a lot of attention in the past [1–8]. The basic idea was to test whether the newly discovered weakly interacting massive particle was consistent with being a thermal relic or not. The general approach was to assume a specific model, most often some version of low-energy supersymmetry, and then attempt to measure all relevant model parameters affecting the thermal relic density calculation. Unfortunately, such an approach is model dependent, applies only to thermal relics (for alternative nonthermal scenarios, see Refs. [9,10]), requires full understanding of the early cosmology, and typically demands a large number of additional measurements, possibly at future (or futuristic) facilities.

Given that *proving* the discovery of dark matter at the LHC is such a difficult task, perhaps one should focus on the opposite question: how to *disprove* that the newly found invisible particle is the cosmological dark matter. One possibility is to perform a precise measurement of its mass, and if the mass is consistent with zero, it may just be one of the Standard Model (SM) neutrinos instead of a brand new particle [11]. However, this logic is not ironclad either: there exist examples where the dark matter particles are very light [12,13] and cannot be ruled out just on the basis of their small mass.

A much more direct approach would be to test whether the particle which is the source of the $\not{E}_T$ is indeed stable; after all, we only know that it did not decay inside the detector. If its lifetime is relatively short, so that it does decay outside, but not too far from the detector, one could attempt to build a dedicated experiment to record such delayed decays. In the past, there were proposals to place such supplementary detectors near the D0 experiment at Fermilab [14] and near the LHC [15], and these ideas were recently revived in Ref. [16]. However, any such experiment is doomed if the dark matter candidate decays invisibly, e.g., to hidden sector particles [17].

In this paper we address the worst-case scenario, when the dark matter candidate produced at the LHC is unstable and decays invisibly. For concreteness, we consider the standard new physics decay chain shown inside the solid box of Fig. 1:

$$A \to v_1 B \to v_1 v_2 C, \tag{1}$$

where $v_{1,2}$ are SM particles (assumed to be massless here for simplicity), while A, B, and C are new particles, with C being the dark matter candidate. The canonical example for

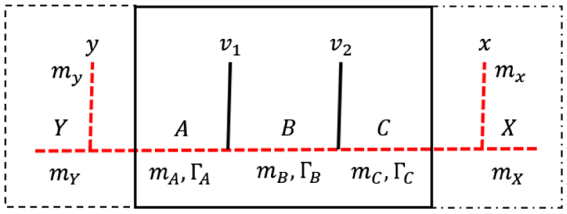

FIG. 1. The new physics decay chain under study.

the processes (1) is the neutralino decay $\tilde{\chi}_2^0 \to \ell\tilde{\ell}^* \to \ell\ell\tilde{\chi}_1^0$ in supersymmetry [18], where $\tilde{\chi}_2^0$ ($\tilde{\chi}_1^0$) is the second-lightest (lightest) neutralino, $\tilde{\ell}$ ($\tilde{\ell}^*$) is a charged (anti)slepton and ℓ ($\bar{\ell}$) is a SM (anti)lepton. The masses of the particles A, B and C are denoted with m_A, m_B and m_C, respectively, and in general all three particles will have corresponding widths Γ_A, Γ_B and Γ_C. In particular, we shall pay special attention to the case when the dark matter "candidate" C is unstable and thus its decay width Γ_C is strictly nonzero. In fact, Γ_C could easily be surprisingly large, e.g., it can be enhanced by the multiplicity of available decay channels for C in the hidden sector. Our key idea here is to attempt a *direct* measurement of the new particle widths (including Γ_C) from the kinematic distributions of the visible decay products v_1 and v_2. If one could unambiguously establish experimentally that $\Gamma_C > 0$, then C will be ruled out as a dark matter candidate. Therefore, our first goal is to derive the effect of nonzero widths on the observable kinematics. In particular, we shall demonstrate as a proof of principle that nonzero particle widths can have an observable impact on the shape of the distribution of the invariant mass $m \equiv m_{v_1 v_2}$ of the two visible particles v_1 and v_2. A more detailed analysis of the exact particle width sensitivity is left for a future study.

II. PURE ON-SHELL CASE

In the purely on-shell case, where all three particles A, B and C are exactly on shell, the distribution dN/dm has the well-known "triangular" shape

$$\frac{dN}{dm} \sim \begin{cases} m/(128\pi^2 m_A^3 m_B \Gamma_B) & \text{for } 0 \le m \le m_{\text{on}}^{\max} m, \\ 0 & \text{otherwise,} \end{cases} \tag{2}$$

which extends up to the kinematic end point $m_{\text{on}}^{\max}$

$$m_{\text{on}}^{\max}(m_A, m_B, m_C) \equiv \sqrt{(m_A^2 - m_B^2)(m_B^2 - m_C^2)}/m_B. \tag{3}$$

The validity of Eq. (2) is ensured (at tree level) as long as the narrow-width approximation holds and there are no significant polarization effects. We shall now investigate how the result (2) is modified in the case of non-negligible widths Γ_A, Γ_B and, most importantly, Γ_C (for studies in other contexts, see Refs. [19–23]). For simplicity, here we shall be turning on those widths one at a time, postponing the discussion of the simultaneous measurement of Γ_A, Γ_B, and Γ_C to a future publication [24].

III. NON-NEGLIGIBLE Γ_B

As a warm-up, we begin with the case when only B is relatively broad, $\Gamma_B \neq 0$. In that case, the narrow-width result (2) gets modified to [25]

$$\frac{dN}{dm} \sim \frac{m}{128\pi^3 m_A^3} \int_{s_-}^{s_+} \frac{ds}{(s - m_B^2)^2 + m_B^2 \Gamma_B^2}, \tag{4}$$

where

$$s_\pm \equiv \frac{1}{2}[m_A^2 + m_C^2 - m^2 \pm \lambda^{1/2}(m_A^2, m_C^2, m^2)], \tag{5}$$

and $\lambda(x, y, z) \equiv x^2 + y^2 + z^2 - 2xy - 2yz - 2xz$. In the limit of massless v_1 and v_2, the lower end point of Eq. (4) is at $m = 0$, while the upper end point, $m_{\Gamma_B}^{\max}$, is obtained by solving the equation $s_- = s_+$, which results in

$$m_{\Gamma_B}^{\max} = m_A - m_C, \tag{6}$$

a result identical to the one for the direct three-body decay

$$A \to v_1 v_2 C. \tag{7}$$

Note that in the narrow-width approximation limit of $\Gamma_B/m_B \to 0$, the integrand in Eq. (4) becomes

$$\lim_{\frac{\Gamma_B}{m_B} \to 0} \frac{1}{(s - m_B^2)^2 + m_B^2 \Gamma_B^2} = \frac{\pi}{m_B^3 \Gamma_B} \delta\left(\frac{s}{m_B^2} - 1\right) \tag{8}$$

and we recover the purely on-shell result (2).

Figure 2 illustrates the effect of a finite-width Γ_B on the invariant mass distribution (4). In general, one should expect sizable effects whenever the width Γ_B is comparable to a relevant mass *splitting*, e.g., $m_A - m_B$ (left panel) or $m_B - m_C$ (right panel). The solid lines depict the invariant

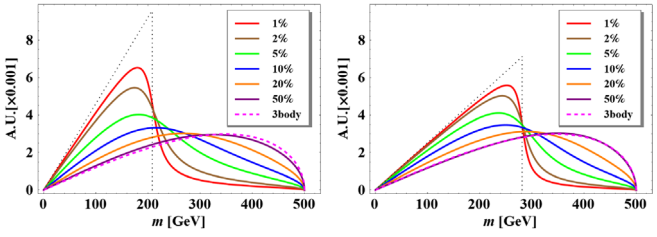

FIG. 2. The solid lines represent unit-normalized invariant mass distributions [Eq. (4)] for $(m_A, m_B, m_C) = (1000, 970, 500)$ GeV (left panel) and $(m_A, m_B, m_C) = (1000, 530, 500)$ GeV (right panel), with negligible Γ_A and Γ_C and several different choices of Γ_B/m_B as shown in the legends. The magenta dashed curve corresponds to the case of a pure three-body decay (e.g., $m_B \gg m_A$).

mass distribution (4) for several different values of Γ_B/m_B, from 1% (red lines) all the way to 50% (purple lines). For comparison, the m distribution for the three-body decay (7) is shown by the magenta dashed curve. We see that initially, as the width Γ_B is relatively small, the shape of the distribution still resembles the triangular shape (indicated by the dotted line) of Eq. (2), but there are a certain number of events which leak out beyond the nominal upper kinematic end point (3). As the width Γ_B increases, so does the fraction of events which leak out, and very soon, for $\Gamma_B/m_B \sim 5$–10%, no discernible end point is visible at all at the location predicted by Eq. (3). Instead, we obtain a relatively broad distribution which terminates at the new kinematic end point (6). Eventually, as the width Γ_B further increases, the distribution asymptotes to the magenta dashed line corresponding to the case of the three-body decay (7).

Figure 2 demonstrates that the effect of a finite Γ_B on the invariant mass distribution (4) can be quite significant; for one, all curves in the figure have shapes which are clearly different from the triangular shape (2) obtained in the limit of $\Gamma_B = 0$. At the same time, unless the B resonance is extremely broad ($\Gamma_B \sim m_B$), the obtained distribution is also distinguishable from that of a three-body decay (7). We thus conclude that the observation of a nontrivial invariant mass shape like the ones seen in Fig. 2 would not only suggest a finite value for Γ_B, but will also allow its measurement with a decent precision.

Before we move on to the case of a non-negligible Γ_C, let us briefly comment on the effect of spin correlations. Our previous results were obtained in the pure phase space limit, where the width dependence comes only from the B propagator. However, these results would be valid only if all involved particles are spin 0, which is unrealistic: the SM particles v_1 and v_2 are fermions (leptons or quark-initiated jets). Therefore, some nontrivial chiralities are present in the interaction vertices, as shown in the left panel

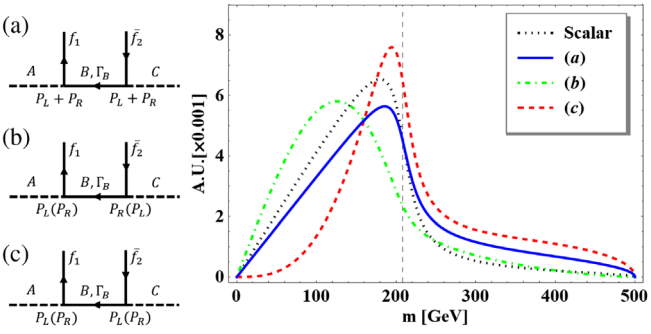

FIG. 3. Left panel: Three different fermion chirality structures for the boxed decay chain of Fig. 1: (a) vectorlike couplings, (b) opposite chiralities, and (c) the same chiralities at the neighboring fermion vertices. Right panel: Unit-normalized invariant mass distributions for those three cases, compared to the pure scalar theory result (4) (black dotted line), for $(m_A, m_B, m_C) = (1000, 970, 500)$ GeV and $\Gamma_B/m_B = 1\%$.

of Fig. 3, where for concreteness we have chosen the intermediate particle B to be a fermion. In general, the fermion couplings are arbitrary mixtures of left-handed and right-handed chiral couplings proportional to $P_L \equiv (1-\gamma_5)/2$ and $P_R \equiv (1+\gamma_5)/2$, respectively. In Fig. 3, we contrast three special cases: (a) vectorlike couplings, (b) opposite chiralities at the two vertices and (c) the same chiralities at the two vertices. Then, the spin-averaged matrix element squared receives an additional contribution proportional to

$$\overline{|\mathcal{M}|^2} \sim \begin{cases} (m_A^2 - s)(s - m_C^2) - m^2 s & \text{for Fig. 3}(b), \\ m^2\left(\dfrac{\Gamma_B^2}{4} + m_B^2\right) & \text{for Fig. 3}(c). \end{cases} \quad (9)$$

Therefore, the result for vectorlike couplings [Fig. 3(a)] is simply the sum of these two cases (times a factor of 2 due to $L \leftrightarrow R$ exchange)

$$\overline{|\mathcal{M}|^2} \sim 2(m_A^2 - s)(s - m_C^2) + 2m^2\left(\frac{\Gamma_B^2}{4} + m_B^2 - s\right). \quad (10)$$

The chirality effects (9)–(10) on the shape of the invariant mass distribution are illustrated in the right panel of Fig. 3, for a mass spectrum $(m_A, m_B, m_C) = (1000, 970, 500)$ GeV and $\Gamma_B/m_B = 1\%$. For reference, the black dotted line shows the pure scalar theory result (4). The green dot-dashed and the red dashed lines represent the distributions obtained in the presence of spin correlations as in Fig. 3(b) and Fig. 3(c), respectively. The case of vectorlike couplings, Fig. 3(a), is then obtained by simply adding those two distributions (blue solid line). In the narrow-width approximation, for vectorlike couplings one would recover the phase space result (2), since the spin correlations from Fig. 3(b) and Fig. 3(c) would cancel exactly. However, in the presence of nontrivial width effects as in Eq. (9), the cancellation is incomplete and even the case of vector-like couplings is markedly different from the pure scalar theory result (compare the blue solid and black dotted lines in Fig. 3) [26,27].

IV. NON-NEGLIGIBLE Γ_C

We now consider perhaps the most interesting case, when the dark matter candidate (particle C) has a non-vanishing width, $\Gamma_C \neq 0$, due to an invisible decay to two dark sector particles X and x, as shown in the right (dot-dashed) boxed extension of Fig. 1. Under those circumstances, we find that the shape of the invariant mass distribution is given by

$$\frac{dN}{dm} \sim \frac{m}{2048\pi^4 m_A^3 m_B \Gamma_B} \int_{s_-}^{s_+} \frac{ds}{s} \frac{\lambda^{1/2}(s, m_X^2, m_x^2)}{(s - m_C^2)^2 + m_C^2 \Gamma_C^2}, \quad (11)$$

where m_X and m_x are the respective masses of the hidden sector particles X and x and

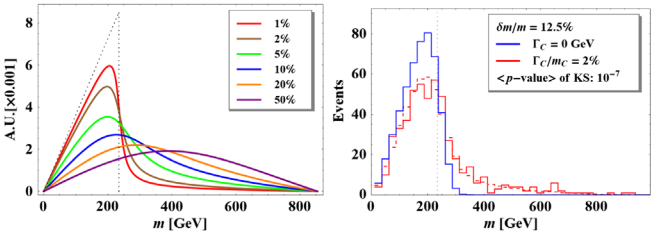

FIG. 4. Left: Unit-normalized invariant mass distributions for $(m_A, m_B, m_C) = (1000, 520, 500)$ GeV and several different values of Γ_C/m_C as shown in the legend. We assume that particle C further decays invisibly to two massless particles X and x, $C \to Xx$, as shown in the dot-dashed box of Fig. 1. Right: the invariant mass distribution of 500 events, after applying Gaussian smearing of 12.5% for the case of $\Gamma_C = 0$ (blue solid line) and $\Gamma_C/m_C = 2\%$ (red solid line). The red dashed line represents the average of 100 pseudoexperiments.

$$s_- \equiv (m_X + m_x)^2, \qquad s_+ \equiv m_B^2\left(1 - \frac{m^2}{m_A^2 - m_B^2}\right). \tag{12}$$

As before, the upper kinematic end point, $m_{\Gamma_C}^{\max}$, of the distribution (11) is found from $s_- = s_+$, which yields

$$m_{\Gamma_C}^{\max} = \sqrt{(m_A^2 - m_B^2)\{m_B^2 - (m_X + m_x)^2\}}/m_B. \tag{13}$$

Comparing to Eq. (3), we notice that

$$m_{\Gamma_C}^{\max} = m_{\rm on}^{\max}(m_A, m_B, m_X + m_x), \tag{14}$$

which is easily understood as the limit when C becomes extremely off shell.

In analogy to Fig. 3, the left panel in Fig. 4 illustrates the impact of the nonvanishing width Γ_C on the shape of the invariant mass distribution (11). We take the mass spectrum to be $(m_A, m_B, m_C) = (1000, 520, 500)$ GeV and again vary the dimensionless ratio Γ_C/m_C from 1% to 50% as indicated in the legend. For concreteness, we assume the hidden sector particles X and x to be massless, i.e., $m_X = m_x = 0$, in which case the distributions in Fig. 4 have a common upper kinematic end point $m_{\Gamma_C}^{\max} = \sqrt{m_A^2 - m_B^2} = 854$ GeV.

Figure 4 demonstrates that the effect of Γ_C can be quite drastic. Even when the width Γ_C is as small as 1% of the resonance mass m_C, the shape of the distribution is visibly distorted from the standard triangular shape (2), and a sizable fraction of events are already leaking out beyond the expected kinematic end point (3), which is indicated with the vertical dashed line. Increasing the width to $\Gamma_C \sim 0.05 m_C$ appears already sufficient to render the triangular shape unrecognizable and indicate the presence of off-shell effects.

In order to test the method in the presence of realistic detector resolution effects, in the right panel of Fig. 4 we plot the invariant mass distribution of 500 events for the worst-case scenario when particles v_1 and v_2 are jets. We apply Gaussian smearing of 12.5%, which is typical for jets, and contrast the cases of $\Gamma_C = 0$ (blue solid line) and $\Gamma_C/m_C = 2\%$ for a single experiment (red solid line) or the average of 100 pseudoexperiments (red dashed line). It is clear that even in the presence of jet smearing, the two cases are easily distinguishable: applying a Kolmogorov-Smirnov test, we find a p-value of 10^{-7} which is sufficient for a 5σ discovery of a nonvanishing Γ_C.

V. NON-NEGLIGIBLE Γ_A

Finally, for completeness we also consider the case where the decay width of particle A is non-negligible, $\Gamma_A \neq 0$. This case is a little bit more model dependent, since we must know how to sample the 4-momentum squared, p_A^2, of particle A. One simple possibility is that A is the decay product of a narrow resonance Y with mass m_Y, $Y \to yA$, as shown in the left (dashed) boxed extension of Fig. 1. Under those circumstances, the invariant mass distribution is given by

$$\frac{dN}{dm} \sim \frac{m}{2048\pi^4 m_Y^3 m_B \Gamma_B}\int_{s_-}^{s_+}\frac{ds}{s}\frac{\lambda^{1/2}(m_Y^2, m_y^2, s)}{(s - m_A^2)^2 + m_A^2\Gamma_A^2}, \tag{15}$$

where m_Y and m_y are the masses of the particles Y and y, respectively, while

$$s_- \equiv m_B^2\left(1 + \frac{m^2}{m_B^2 - m_C^2}\right), \qquad s_+ \equiv (m_Y - m_y)^2. \tag{16}$$

The upper kinematic end point, $m_{\Gamma_A}^{\max}$, of the distribution (15) is again found from $s_- = s_+$:

$$m_{\Gamma_A}^{\max} = \sqrt{\{(m_Y - m_y)^2 - m_B^2)(m_B^2 - m_C)^2}/m_B, \tag{17}$$

and can be equivalently interpreted as

$$m_{\Gamma_A}^{\max} = m_{\rm on}^{\max}(m_Y - m_y, m_B, m_C). \tag{18}$$

Figure 5 shows the effect of a nonvanishing width Γ_A on the shape of the invariant mass distribution (15). The mass spectrum is chosen as $(m_Y, m_A, m_B, m_C) = (1500, 1000, 970, 500)$ GeV and the dimensionless ratio Γ_A/m_A is again varied from 1% to 50%, as indicated in the legend. For concreteness, we assume that the additional final-state particle y is massless, and thus all distributions in Fig. 5 have a common kinematic end point $m_{\rm on}^{\max}(m_Y, m_B, m_C) = 980$ GeV, as predicted by Eq. (18). Once again, we observe that even a width of only 1% leads to a noticeable change in the expected triangular shape and an overflow of events beyond the nominal kinematic end point of 208.3 GeV predicted by Eq. (3) and denoted by the vertical dashed line. As the width is further increased,

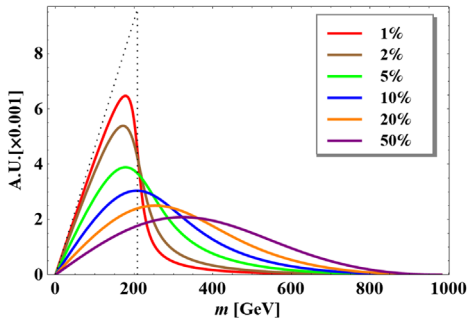

FIG. 5. Unit-normalized invariant mass distributions for $(m_Y, m_A, m_B, m_C) = (1500, 1000, 970, 500)$ GeV and several different values of Γ_A/m_A as shown in the legend. We assume that A results from the decay of a parent particle Y, $Y \to yA$ (see the dashed box of Fig. 1). The particle y is assumed massless, and may or may not be visible in the detector.

the shape distortion becomes quite significant, confirming the sensitivity to the value of Γ_A.

VI. SUMMARY AND OUTLOOK

We derived the effects of nonzero particle widths on the observable invariant mass distribution dN/dm in the case of the decay chain of Fig. 1. We showed that the shape of the distribution can be very sensitive to the widths and therefore can be used to perform a measurement of Γ_A, Γ_B and, most importantly, Γ_C, thus directly probing the nature of the dark matter candidate C, which appears invisible in the detector. Our results for these three cases can be compactly summarized as

$$\frac{dN}{dm} \sim m \int_{s_{i-}}^{s_{i+}} ds \frac{1}{(s-m_i^2)^2 + m_i^2\Gamma_i^2} F_i(s), \qquad (19)$$

where $i = \{A, B, C\}$, the integration limits $s_{i\pm}$ are given by Eqs. (16), (5) and (12), respectively, while

$$F_i(s) = \begin{cases} \dfrac{\lambda^{1/2}(m_Y^2, m_y^2, s)}{s} & \text{for } i = A, \\ 1 & \text{for } i = B, \\ \dfrac{\lambda^{1/2}(s, m_X^2, m_x^2)}{s} & \text{for } i = C. \end{cases} \qquad (20)$$

The analysis presented here can be readily generalized to the case of massive SM particles v_1 and v_2, to three-body decays, and to a simultaneous measurement of Γ_A, Γ_B and Γ_C [24].

One should be mindful of the fact that there are other factors which also affect the shape of the invariant mass distribution dN/dm. On the theoretical side, there could be spin correlations [26,28–30], interference [31,32] and higher-order effects [33,34]. On the experimental side, the analysis cuts, the detector resolution, and the SM backgrounds will also play roles in this measurement. However, these effects are well known and under control, and can be readily accounted for (see, e.g., the kinematic end point measurements in Ref. [35]). Furthermore, the width measurement relies mostly on the events *above* the nominal kinematic end point (3), while all those effects impact mostly the softer part of the distribution dN/dm. We are therefore optimistic that such width measurements will be feasible, once a sufficiently strong and clean missing energy signal of new physics is observed at the LHC.

ACKNOWLEDGMENTS

We would like to thank Gennaro Corcella and Rakhi Mahbubani for insightful discussions. This work is supported in part by a U.S. Department of Energy Grant No. DE-SC0010296. D. K. was supported in part by the LHC Theory Initiative postdoctoral fellowship (NSF Grant No. PHY-0969510), and is presently supported by the Korean Research Foundation (KRF) through the CERN-Korea Fellowship program.

[1] M. Battaglia, I. Hinchliffe, and D. Tovey, Cold dark matter and the LHC, J. Phys. G **30**, R217 (2004).
[2] B. C. Allanach, G. Belanger, F. Boudjema, and A. Pukhov, Requirements on collider data to match the precision of WMAP on supersymmetric dark matter, J. High Energy Phys. 12 (2004) 020.
[3] J. L. Bourjaily and G. L. Kane, What is the cosmological significance of a discovery of WIMPs at colliders or in direct experiments?, arXiv:hep-ph/0501262.
[4] T. Moroi, Y. Shimizu, and A. Yotsuyanagi, Reconstructing dark matter density with e^+e^- linear collider in focus-point supersymmetry, Phys. Lett. B **625**, 79 (2005).
[5] A. Birkedal *et al.*, Testing cosmology at the ILC, *2005 International Linear Collider 351 Workshop, Stanford, CA, 2005*, eConf C050318, 0708 (2005).
[6] M. M. Nojiri, G. Polesello, and D. R. Tovey, Constraining dark matter in the MSSM at the LHC, J. High Energy Phys. 03 (2006) 063.
[7] E. A. Baltz, M. Battaglia, M. E. Peskin, and T. Wizansky, Determination of dark matter properties at high-energy colliders, Phys. Rev. D **74**, 103521 (2006).
[8] D. Chung, L. Everett, K. Kong, and K. T. Matchev, Connecting LHC, ILC, and Quintessence, J. High Energy Phys. 10 (2007) 016.

[9] J. L. Feng, A. Rajaraman, and F. Takayama, SuperWIMP dark matter signals from the early universe, Phys. Rev. D **68**, 063504 (2003).
[10] H. Baer, K. Y. Choi, J. E. Kim, and L. Roszkowski, Dark matter production in the early Universe: Beyond the thermal WIMP paradigm, Phys. Rep. **555**, 1 (2015).
[11] S. Chang and A. de Gouvea, Neutrino alternatives for missing energy events at colliders, Phys. Rev. D **80**, 015008 (2009).
[12] J. F. Gunion, D. Hooper, and B. McElrath, Light neutralino dark matter in the NMSSM, Phys. Rev. D **73**, 015011 (2006).
[13] H. K. Dreiner, S. Heinemeyer, O. Kittel, U. Langenfeld, A. M. Weber, and G. Weiglein, Mass bounds on a very light neutralino, Eur. Phys. J. C **62**, 547 (2009).
[14] C. H. Chen and J. F. Gunion, Probing gauge mediated supersymmetry breaking models at the Tevatron via delayed decays of the lightest neutralino, Phys. Rev. D **58**, 075005 (1998).
[15] K. Maki and S. Orito, Hadron colliders as the "neutralino factory": Search for a slow decay of the lightest neutralino at the CERN LHC, Phys. Rev. D **57**, 554 (1998).
[16] J. P. Chou, D. Curtin, and H. J. Lubatti, New detectors to explore the lifetime frontier, Phys. Lett. B **767**, 29 (2017).
[17] M. J. Strassler, Possible effects of a hidden valley on supersymmetric phenomenology, arXiv:hep-ph/0607160.
[18] I. Hinchliffe, F. E. Paige, M. D. Shapiro, J. Soderqvist, and W. Yao, Precision SUSY measurements at CERN LHC, Phys. Rev. D **55**, 5520 (1997).
[19] G. Mahlon and S. J. Parke, Finite width effects in top quark decays, Phys. Lett. B **347**, 394 (1995).
[20] J. A. Oller, Finite width effects in phi radiative decays, Nucl. Phys. **A714**, 161 (2003).
[21] T. Han, I. W. Kim, and J. Song, Kinematic cusps with two missing particles II: Cascade decay topology, Phys. Rev. D **87**, 035004 (2013).
[22] P. Falgari, A. S. Papanastasiou, and A. Signer, Finite-width effects in unstable-particle production at hadron colliders, J. High Energy Phys. 05 (2013) 156.
[23] S. Moretti, D. O'Brien, L. Panizzi, and H. Prager, Production of extra quarks decaying to dark matter beyond the narrow width approximation at the LHC, Phys. Rev. D **96**, 035033 (2017).
[24] D. Kim and K. Matchev (to be published).
[25] Y. Grossman, M. Martone, and D. J. Robinson, Kinematic edges with flavor oscillation and non-zero widths, J. High Energy Phys. 10 (2011) 127.
[26] L. T. Wang and I. Yavin, Spin measurements in cascade decays at the LHC, J. High Energy Phys. 04 (2007) 032.
[27] D. Berdine, N. Kauer, and D. Rainwater, Breakdown of the narrow width approximation for new physics, Phys. Rev. Lett. **99**, 111601 (2007).
[28] A. J. Barr, Determining the spin of supersymmetric particles at the LHC using lepton charge asymmetry, Phys. Lett. B **596**, 205 (2004).
[29] J. M. Smillie and B. R. Webber, Distinguishing spins in supersymmetric and universal extra dimension models at the large hadron collider, J. High Energy Phys. 10 (2005) 069.
[30] M. Burns, K. Kong, K. T. Matchev, and M. Park, A general method for model-independent measurements of particle spins, couplings and mixing angles in cascade decays with missing energy at hadron colliders, J. High Energy Phys. 10 (2008) 081.
[31] A. Birkedal, R. C. Group, and K. Matchev, Slepton mass measurements at the LHC, *2005 International Linear Collider Workshop, Stanford, CA, 2005*, eConf C050318, 0210 (2005).
[32] E. Fuchs, S. Thewes, and G. Weiglein, Interference effects in BSM processes with a generalised narrow-width approximation, Eur. Phys. J. C **75**, 254 (2015).
[33] M. Drees, W. Hollik, and Q. Xu, One-loop calculations of the decay of the next-to-lightest neutralino in the MSSM, J. High Energy Phys. 02 (2007) 032.
[34] M. Beneke, L. Jenniches, A. Mck, and M. Ubiali, Radiative distortion of kinematic edges in cascade decays, Phys. Lett. B **770**, 539 (2017).
[35] S. Chatrchyan *et al.* (CMS Collaboration), Measurement of masses in the $t\bar{t}$ system by kinematic endpoints in pp collisions at $\sqrt{s} = 7$ TeV, Eur. Phys. J. C **73**, 2494 (2013).